*Eco. Env. & Cons. 27 (May Suppl. Issue) : 2021; pp. (S42-S47)*
*Copyright@ EM International*
*ISSN 0971–765X*

# Sensible heat flux characterization using satellite remote sensing techniques

**Uma Devi Randhi[1]*, J. Swaraj[2], K. Suresh Kumar[3] and T.B. Patrudu[1]**

*[1] GITAM Deemed to be University, School of Science, Hyderabad, Telangana State, India*
*[2] Environmental Pollution Training and Research Institute (EPTRI), Hyderabad, India*
*[3] GITAM Deemed to be University, Institute of Science, Visakhapatnam, Andhra Pradesh State, India*

(Received 27 September, 2020; Accepted 9 November, 2020)

**ABSTRACT**

Land surface temperature (LST), vegetation index, and emissivity are significant heat flux calculating components. These also stand as critical indicators for environmental components analysis in the climatological, meteorological, and hydrological applications. In this study, extensive research illustrated heat flux characterization by generating land surface temperature (LST) with LANDSAT - 8 satellite images for Patancheru industrial area subjected to algorithm-based analysis. A simultaneous Land use Land cover (LULC) classification developed for different category areas such as vegetation, bare soil, water body, and built-up land. These classes zonal attributes were calculated from the various developed products such as emissivity, Land surface temperature (LST), and Sensible heat flux. From the results, the emissivity values observed are in the range between 0.98 and 0.99. The LST values are observed in between 30 to 44 $^{o}$C. A high SHF value was found over the Gullied areas as 17.2815 W/m$^2$, followed by industrial area (3.8508 W/m$^2$) and built-up land (-2.8161 W/m$^2$). Multi-temporal data helped to investigate the relationship between land surface temperature (LST) and normalized difference vegetation index (NDVI) values in temporal resolution. These results represented the high-temperature variations in the study area. The sensible heat flux characterization results proved that sensible heat flux and land surface temperature values are directly proportional.

***Key words:*** *Emissivity, Vegetation index, Heat flux, Land use/Land cover and Land surface temperature.*

## Introduction

Land cover dynamics like normalized difference vegetation index (NDVI), land surface temperature (LST), and emissivity, etc. have been developing and validating for various studies using Remote sensing imagery (French *et al.,* 2002; Thomas *et al.,* 2007). The anthropogenic activities which tend to more urbanization and drastic changes in the land use patterns are altering the climatic conditions (Md. Bodruddoza *et al.,* 2012). These problems are creating more impacts in the urban areas than the rural areas (Tatygul, 2017). The conversion of vegetated surfaces in the urban areas into the impervious imparting the high surface temperatures. These changes show an impact on surface temperature rises and offer more evaporation rates, heat storage by high solar radiation absorbance, and more wind turbulences. These are altering the surface atmospheric conditions, mainly in the urban areas (Sundara *et al.,* 2012). Generally, the difference in

**Abbreviations**
LULC, land use land cover; NDVI, normalized difference vegetation index; LST, land surface temperature; TOA, Top of Atmospheric spectral radiance.

temperature between urban and rural settlements is called urban heat island (UHI). UHI's temperatures lead to disturbances in local hydrological patterns, a rise in pollution levels, and a rise in air conditioning demands.

Hyderabad is a rapidly growing urban area with more migrations by people due to developmental activities and employment facilities. These urban sprawl conditions are severely affecting the biophysical environment. So, urban sprawl and unplanned urbanization are severely affecting the land use patterns (Tamilenthi *et al*., 2011). These LULC changes resemble the increase in a barren area, deforested area, loss of agricultural lands, increases impermeable surface structures, and finally, results with high surface temperatures. Many studies evaluated the urban area's relative warmth by land-based observation methods and air temperature sensors (Yamashita, 1996). But these methods are time-consuming and expensive. Spatial remote sensing techniques proved to be a better alternative method to the practices described above due to high resolution and the capability to cover and measure the earth's surface conditions (Simwanda *et al.*, 2019). These techniques are useful in calculating the urban heat island effect quickly. In the present study, surface emissivity and land surface temperature were evaluated to characterize sensible heat flux by using spatial techniques.

### Study Area

Patancheru industrial area is located in the Northwest direction to the Hyderabad at 17°31′43.47"N latitude and 78°16′0.21"E longitude. It is considered as the significant and most polluted industrial area of Hyderabad in Telangana State, India. Several kinds of research proved that the Patancheru industrial area contained the highest level of drug pollution in water resources (Christoph *et al*., 2017). Along with water pollution, air pollution is also severe in this area due to industries and more vehicle density. The satellite image of the Patancheru industrial area is presented in Figure 1.

## Methodology

### Data Used

The satellite of Landsat 8 is an American Earth observation satellite. It was launched on 11th February 2013, and it is the collaborated satellite between the

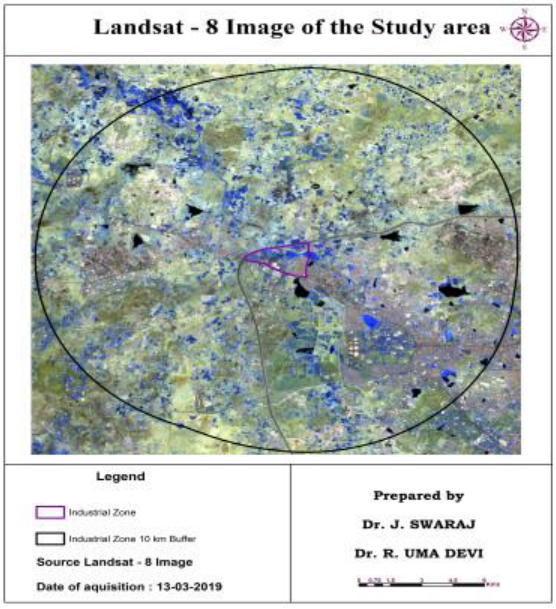


**Fig. 1.** Study area image from Landsat satellite.

NASA and United States Geological Survey (USGS). It is also called a Landsat continuity Mission (LDCM). Table 1 represents the Landsat satellite data details. The ancillary meteorological data from the websites: http://www.mosdac.gov.in, www.wunder ground.com, are collected and used.

A generalized split-window algorithm applied for the estimation of surface land temperatures by several researchers (Javed *et al.*, 2008). Quantification of various factors is required from satellite data to assess land surface temperature (LST) accurately. It contains the spatial variability characterization for land cover along with the sensor radiometric calibrations. The fractional vegetative cover, atmospheric correction, surface emissivity correction, and combined effects of geometry are also considered for assessing accuracy. Along with these, various tools of ENVI, Arc Map, and ERDAS soft ware's applied for the analysis of complete study data. An additive rescaling factor and Band specific multiplicative rescaling factors from the metadata are used for the calculation of the Top of Atmospheric spec-

**Table 1.** Landsat satellite Data details.

| S.No | Month | March |
|---|---|---|
| 1 | Satellite | Landsat 8 |
| 2 | Sensor | OLI and TIRS |
| 3 | Date of Acquisition | 13/12/2019 |
| 4 | Path | 146 |
| 5 | Row | 40 |

tral radiance (TOA) (Franzpc, 2019; Li *et al.,* 2018). It contains the spatial variability characterization for land cover along with the formula for this calculation is

$$TOA\ (L) = ML * Qcal + AL \quad .. (1)$$

Here, AL is considered as Band-specific additive rescaling factor, Q corresponds to band 10, and ML refers to Band-specific multiplicative rescaling factor.

Therefore

$$TOA = 0.10033*B \text{ and } 10 + 0.1 \quad .. (2)$$

Based on this, the Brightness temperature is framed through converting of TOA.

$$BT = (K2 / (\ln (K\ 1 / L) + 1)) - 273.15 \quad .. (3)$$

Where K1, K2 refers to the constants of Band specific thermal conversions from metadata.

Hence,

$$\text{Brightness Temperature (BT)} = (1321.0789/ \text{Ln}((774.8853/TOA)+1)) - 273.15 \quad .. (4)$$

Now, NDVI calculation is essential as it gives the vegetation proportions(P) in the study area and also emissivity (ε).

$$NDVI = (Band\ 5 - Band\ 4) / (Band\ 5 + Band\ 4) \quad .. (5)$$

Based on this equation (5), the vegetation Pv proportions are calculated with the following equations.

$$P\ v = Square\ ((NDVI - NDVImin)/(NDVImax - NDVImin)) \quad .. (6)$$

$$Pv = Square((NDVI - 0.0445224)/(0.339563 - .0445224)) \quad .. (7)$$

Based on these vegetation Pv proportions, the emissivity is calculated with the following equation.

$$\varepsilon = 0.004 \times Pv + 0.986 \quad .. (8)$$

Here, 0.986 values is considered as the equation correction value.

**Analysis of the Land Surface Temperature (LST)**

Spectral radiance was analyzed by converting the image pixels digital number (DN) from the satellite thermal data and the sensor calibration data. Accurate surface temperature is not represented by only the radiation derived based on the digital number. But it represents along with the different energy fractions and mixed signals. These energy fractions are present in the hemisphere in the form of upwelling and down welling radiances and emitted energy from the ground (Bromley *et al.,* 2011). So, the LST requires the correction of both atmospheres as well as surface emissivity. Here, LST's measurement requires the NDVI concerning different categories such as bare ground, a mixture of bare soil, vegetation, and, finally, fully vegetation using a subsequent algorithm.

$$LST = (BT/(1 + (0.00115 * BT/1.4388) * Ln(å))) \quad (9)$$

This equation is applied to the generation of surface temperature maps.

**Calculation of Heat Flux**

The energy transferred between the atmosphere and the surface when the temperature differences have occurred is referred as sensible heat (Li, 2018). It can be computed using the bulk aerodynamic method, which is expressed as

$$H = r_a x Cp\ (LST - Temp)/r_{ah} \quad .. (10)$$

where $C_P$ resembles specific heat capacity of air (1004 J/Kg), $r_a$ depicts the density of air and $r_{ah}$ stands for aerodynamic resistance to heat transfer.

## Results and Discussion

Spatial analyses are done to create maps and also to study the relationships of derived parameters. In this study, spatial image maps were generated instead of key maps as these only suit for calculation of emissivity and heat flux. Figure 2 depicts the study area's Land use classification image. Based on the results, Land use classification clearly shows that the residential areas (low dense and high dense built-up) are present in the south and eastern part. Agricultural lands are mostly present in the south

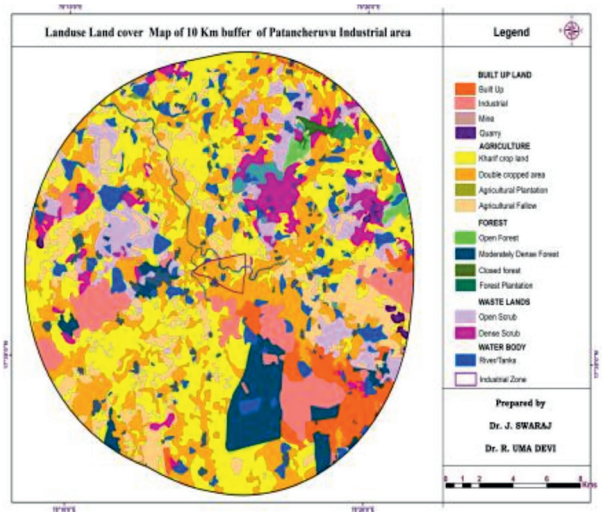


**Fig. 2.** Land use classification.

and north-western part. Water bodies and forests are found in the north-east part in the study area, and most of the industrial areas are present in the east, west, and south parts of the study area. In this, 216.49 hectares of agricultural land is present with a double-cropping pattern, and 4.89 hectares of agricultural land with a single cropping pattern is identified. Water bodies are present in 3.23 hectares, and built up-Industrial land is occupied in 69.25 hectares and 61.89 hectares of the Built-up - Compact (continuous) area.

**Emissivity of the study area**

The objects which have temperatures more than absolute zero emits the thermal radiation (TR). The amount of thermal radiation emitted for a particular temperature and wavelength depends on the emissivity of that specific object surface (Meng *et al*., 2019). Generally, the emissivity of a surface controls various factors such as roughness structure, chemical composition, water content, etc. Emissivity also varies for vegetated surfaces based on the stage of growth, aerial density, and plant species variety. Hence, the ratio between the actual radiance emitted by a real-world selective radiating body and the same thermodynamic temperature released by a black body is emissivity (Srivastava *et al*., 2010; Malakar *et al.*, 2018). This results shown the surface emissivity in five categories, i.e. agricultural land with single and double cropping patterns, water bodies, built-up land and industrial built-up area (Figure 3). The reference sources of the black body use for the calibration of Radiation thermometers usually have an emissivity close to 1. It generally

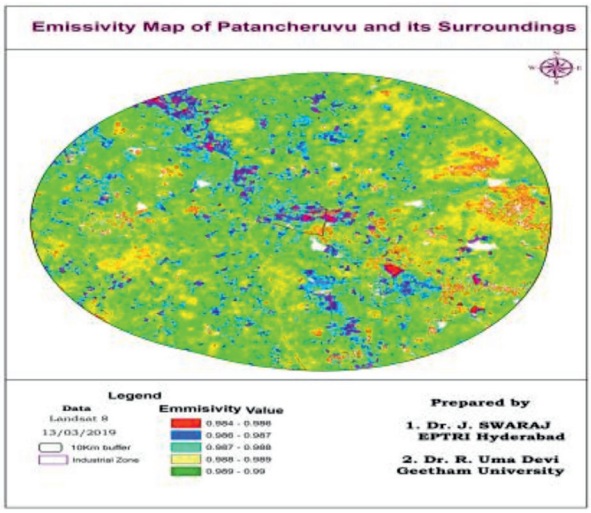


**Fig. 3.** Showing emissivity in the study area.

makes not that much practical difference. But it is considered as a dimensionless number between 0 and 1 concerning perfect reflector and emitter.

**Land Surface Temperature (LST) of the study area**

The map of LST during the year 2019 for the study area is shown in Figure 4. From this, the highest values of LST have indicated the bare soil, quarries, high dense built-up areas, and ash mounds. In contrast, lower land surface temperatures (except water bodies) have stated the vegetative areas, higher NDVI values (agriculture, forest) observed areas.

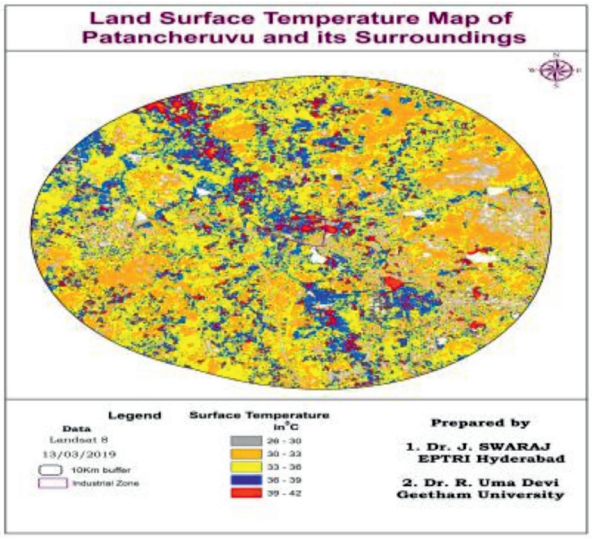


**Fig. 4.** Land Surface Temperature of the study area.

**Evaluation of Sensible Heat Flux**

In this study, the heat flux analysis indicated considerable differences between the native vegetation, water bodies, and irrigated plots concerning emissivity values. Various types of land use differences with high degrees obtained from LST's image in the study area. The obtained NDVI values from the images were used to analyze the emissivity. The emissivity values observed are in the range between 0.98 and 0.99 from the emissivity maps. The LST assessment result shows that LST values are observed from 30 to 44 °C. Figure 5 depicts the sensible heat flux (SHF) image of the present study area. Sensible heat flux (SHF) values during December 2019 were found to vary between -36 and 17 W/m$^2$. A high SHF value was found over the Gullied areas as 17.2815 W/m$^2$, followed by industrial area (3.8508 W/m$^2$) and built-up land (-2.8161 W/m$^2$ ). And the lower values are observed over water bodies/

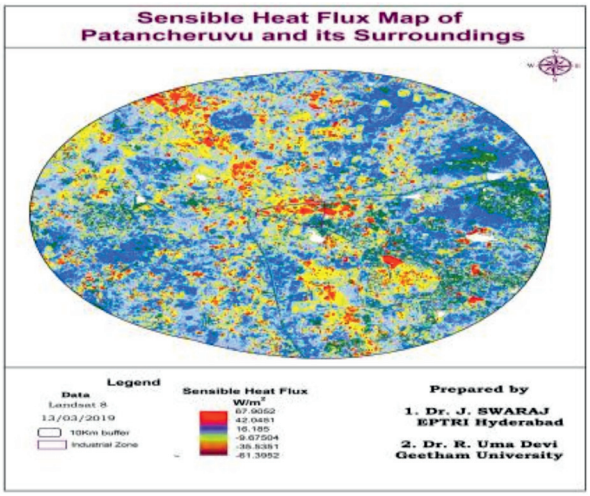


**Fig. 5.** Sensible Heat Flux.

marshy areas and vegetation areas. The areas with good vegetation like the cropped area, plantation, forest, and water bodies are indicated with lower LST and SHF values. Zhou et al. (2018) also stated that the vegetation and water bodies emit lower sensible heat flux values than built-up areas. Table 2 shows the details of classification on individual parameters.

## Conclusison

In this study, the heat flux analysis indicated considerable differences between the native vegetation, water bodies, and irrigated plots concerning emissivity values. Various types of land use differences with high degrees obtained from LST's image in the study area. The obtained NDVI values from the images were used to analyze the emissivity. The emissivity values observed are in the range between 0.98 and 0.99 from the emissivity maps. The LST assessment result shows that LST values are observed from 30 to 44 $^{o}$C. The areas of gullies, highly dense built-up regions indicated with higher levels along with quarries followed by bare soil, which are generally exposed without any vegetation/crop. The results showed that sensible heat flux (SHF) and LST's characterization depend on the emissivity values of land surface features. According to the land surface temperature map, Gullied areas, high dense built-up areas have more surface temperature than the low dense built-up areas. Sensible heat flux values are derived by using temperature values over LULC classes from the study area. From this, it is observed that sensible heat flux and land surface temperature values are directly proportional. A high SHF value was found over the Gullied areas as 17.2815 W/m$^2$, followed by industrial area (3.8508 W/m$^2$) and built-up land (-2.8161 W/m$^2$). Multitemporal data helped to analyze the relationship of LST as well as NDVI values in temporal resolution. Due to urbanization and continuous developmental activities, most of the land in the study area is present with gullies and impervious materials such as concrete and asphalt. With the lack of vegetation in these areas, more heat is generating than the surrounding rural areas. These results represented the high-temperature variations in the study area, and also these results can be used to enhance the quality of the environment, better urban planning to reduce the urban heat island effect.

**Table 2.** Showing the detailed Heat flux values.

| LULC_NAME | LULC (in HC) | Emissivity | Sensible Heat Flux (W/m$^2$) | Land Surface Temp in $^{0}$C |
|---|---|---|---|---|
| Barren Land | 23.0759 | 0.9883 | -8.0044 | 41.4283 |
| Built Up Land | 15.7335 | 0.9880 | -2.8161 | 42.5486 |
| Double Crop | 197.3801 | 0.9887 | -34.2455 | 30.8491 |
| Gullied | 227.9309 | 0.9866 | 17.2815 | 44.5870 |
| Industrial Area | 18.1499 | 0.9879 | 3.8508 | 43.9103 |
| Lake/Pond/Reservoir/Tank | 1.5543 | 0.9881 | -24.6333 | 31.7472 |
| Land With or Without Scrub | 258.6257 | 0.9879 | -19.3319 | 32.2215 |
| Lay outs | 18.4746 | 0.9878 | -12.8761 | 37.1849 |
| Plantations | 5.3847 | 0.9888 | -34.9850 | 30.7910 |
| River/Canal/Drain | 114.6701 | 0.9880 | -29.3703 | 31.3028 |
| Sandy Area - Riverine | 16.7387 | 0.9859 | -41.1672 | 30.2167 |
| Scrub Forest | 62.7163 | 0.9883 | -36.3155 | 30.6650 |
| Scrub Land | 49.1696 | 0.9881 | -22.5704 | 31.9331 |

## References


Bromley, C. J., Manen, S. M. and Mannington, W. 2011. Heat flux from steaming ground: reducing uncertainties. *Proceedings Thirty-Sixth Workshop on Geothermal Reservoir Engineering Stanford University, Stanford, California*.

Christoph Lubbert, Christian Baars, Anil Dayakar, Norman Lippmann, Arne C. Rodloff, Martina Kinzig and Fritz Sörgel. 2017. Environmental pollution with antimicrobial agents from bulk drug manufacturing industries in Hyderabad, South India, is associated with dissemination of extended spectrum betalactamase and carbapenemase producing pathogens. *Infection*, DOI: 10.1007/s15010-017-1007-2.

Franzpc. 2019. How to calculate Land Surface Temperature with Landsat 8 satellite images. Geo Geek in GIS.

French, A.N., Schmugge, T.J., Kustas, W.P., Brubaker, K.L. and Prueger, J. 2002. Surface energy fluxes over El Reno, Oklahoma, using high-resolution remotely sensed data. *Water Resources Research.* 39 (6) : 1164.

Javed Mallik, Yogesh Kant and Bharath, B.D. 2008. Estimation of land surface temperature over Delhi using landsat-7 ETM+. *J. Ind. Geophysics Union*. 2 (3) : 131-140.

Li, S. and Jiang, G.M. 2018. Land surface temperature retrieval from Landsat-8 data with the generalized split-window algorithm. *IEEE Access.* 6 : 18149–18162.

Malakar, N.K., Hulley, G.C.,Hook, S.J., Laraby, K., Cook, M. and Schott, J.R. 2018. An operational land surface temperature product for Landsat thermal data: Methodology and validation. *IEEE Trans. Geosci. Remote Sens*. 56 : 5717–5735.

Md. Bodruddoza Mia, Chris J. Bromley and Yasuhiro Fujimitsu. 2012. Heat flux monitoring using satellite based imagery at Karapiti (craters of the moon) Fumarole area, Taupo. New Zealand.

Meng, X., Cheng, J., Zhao, S., Liu, S. and Yao, Y. 2019. Estimating land surface temperature from Landsat-8 data using the NOAA JPSS enterprise algorithm. *Remote Sens.* 11 : 155.

Simwanda, M., Ranagalage, M., Estoque, R.C. and Murayama, Y. 2019. Spatial analysis of surface urban heat islands in four rapidly growing African cities. *Remote Sens.* 11 : 1645.

Srivastava, P. K., Majumdar, T. J. and Bhattacharya, K. Amit. 2010. Study of land surface temperature and spectral emissivity using multi sensor satellite data. *J. Earth Syst. Sci.* 119 (1) : 67–74.

Sundara Kumar, K., Udaya Bhaskar, P. and Padmakumari, K. 2012. Estimation of land surfacetemperature to study urban heat island effect using Landsat ETM + *image*. *International Journal of Engineering Science and Technology (IJEST).* 4 : 771-778.

Tamilenthi, S., Punithavathi, J., Baskaran, R. and Chandra Mohan, K. 2011. Dynamics of urban sprawl, changing direction and mapping: A case study of Salem city, Tamilnadu, India. *Achieves of Applied Science Research*. 3 (1) : 277-286.

Tatygul Urmambetova. 2017. Characterization of Surface Heat Fluxes over Heterogeneous Areas Using Landsat 8 Data for Urban Planning Studies. Centre for Research on Settlements and Urbanism. *Journal of Settlements and Spatial Planning.* 8 : 49-58.

Thomas M Lillesand, Ralph W. Keifer and Jonathan W. Chipman. 2007. *Remote Sensing and Image Interpretation.* Chapter : 5. John Wiley & Sons (Asia) Pvt. Ltd. Singapore.

Yamashita. 1996. Detail Structure of Heat Island Phenomena from Moving Observations from Electric Trans Cars in Metropolitan Tokyo. *Atmospheric Environment*. 30 : 429-435.

Zhou, D., Xiao, J., Bonafoni, S., Berger, C., Deilami, K., Zhou, Y., Frolking, S., Yao, R., Qiao, Z. and Sobrino, J. 2018. Satellite remote sensing of surface urban heat islands: Progress, challenges, and perspectives. *Remote Sens.* 11 : 48.